

Identification for Nonlinear Flow Characteristics of Main Steam Regulating Valves in Power Plants by Mining Special Data Segments

Xiaotong Xing^{ID}, Jiandong Wang^{ID}, Senior Member, IEEE, Peng Wei^{ID}, Song Gao^{ID}, and Xiangkun Pang^{ID}

Abstract—Nonlinear flow characteristics of main steam regulating valves play an important role on the performance of primary frequency control in thermal power generation units. Manual testing is a traditional method to capture nonlinear flow characteristics by maintaining constant steam pressures, changing control valve openings, and observing power output changes; however, such a method disturbs normal operations of power generation units. This article proposes a new method to identify nonlinear flow characteristics of main steam regulating valves by exploiting special segments hidden in historical operating data. The special segments refer to steady-state segments with constant amplitudes and slope-response segments with large amplitude changes, both of which can be automatically extracted from historical operating data. Relationships between the special segments and a nonlinear model of flow characteristics are theoretically established, and unknown model parameters are estimated by a linear dynamic programming algorithm. These special segments can separate the nonlinear flow characteristics of regulating valves from dynamic effects of steam turbines and generators at different operating points. The necessity of such a separation is demonstrated by a comparison with the Hammerstein model identification method and the sparse identification method. The identified model can be visually verified by comparing measured outputs in the extracted special segments with simulated model outputs. Industrial case studies demonstrate the effectiveness of the proposed method.

Index Terms—Hammerstein models, historical operating data, main steam regulating valves, nonlinear flow characteristics.

Manuscript received 29 May 2023; revised 19 December 2023; accepted 7 February 2024. Date of publication 5 March 2024; date of current version 6 May 2024. This work was supported in part by the National Natural Science Foundation of China under Grant 62273215, and in part by the Research Fund for Taishan Scholar Project of Shandong Province in China. Paper no. TII-23-1917. (Corresponding author: Jiandong Wang.)

Xiaotong Xing, Jiandong Wang, and Peng Wei are with the College of Electrical Engineering and Automation, Shandong University of Science and Technology, Qingdao 266510, China (e-mail: xingxiaotong@163.com; jiandong@sdu.edu.cn; weipeng_0808@163.com).

Song Gao and Xiangkun Pang are with the Shandong Electric Power Research Institute for State Grid Corporation of China, Jinan 250003, China (e-mail: gaosong@yjj.sgcc.com.cn; pangxiangkun@yjj.sgcc.com.cn).

Color versions of one or more figures in this article are available at <https://doi.org/10.1109/TII.2024.3366250>.

Digital Object Identifier 10.1109/TII.2024.3366250

I. INTRODUCTION

WITH the increasing amount of renewable energies in smart grids, higher requirements have been put forward for the operational flexibility of thermal power generation units [1], [2]. Specifically, power generation units should have the ability to adjust power generation frequently and quickly in a wide range for suppressing the power grid frequency fluctuations, and maintaining the balance of power supply and consumption in power grids [3]. A main way of power generation adjustment is primary frequency control, which is realized by controlling the openings of regulating valves to change the main steam flow [4]. The relationship between the valve opening and steam flow is referred to as the flow characteristics of main steam regulating valves. The flow characteristics may become nonlinear due to many factors such as equipments aging. Nonlinear flow characteristics may lead to poor control performance that the generated power cannot respond quickly and completely to a load command, resulting in reduced flexible capacities of power generation units.

The identification of flow characteristics of main steam regulating valves has attracted persisting attention from engineers and researchers [5], [6], [7]. In order to reduce the throttling loss, direct measurement devices of the main steam flow are usually not installed in power generation units. A traditional method for obtaining flow characteristics is based on manual tests [8], [9]. The main steps are to manually increase regulating valve openings under the condition of keeping the main steam pressure at a constant value, and record the corresponding measurements of generated power and valve position. The manual tests require restrictive conditions of maintaining a constant main steam pressure, and need to be repeated at different opening positions of regulating valves. As a result, the manual tests are very time consuming and will disturb normal operations of power generation units.

Flow characteristics of main steam regulating valves can also be estimated by Hammerstein model identification methods [10], [11], [12] and sparse identification methods [13], [14], [15]. Hammerstein models consist of a static nonlinearity block followed by a linear dynamic block, which describe the flow characteristics of regulating valves and the dynamics of steam turbines and generators, respectively. There are quite a few identification methods for Hammerstein mod-

els [16], such as the over-parameter method [17], the subspace identification method [18], and the multiple source signal method [19]. Sparse identification methods introduce a library containing large candidate nonlinear functions, and select a few appropriate functions in the library to describe nonlinear static and dynamic models [20], [21]. However, when the generated power varies greatly, the dynamics of steam turbines and generators are significantly different [22]. The changing dynamic characteristics are mixed with the nonlinear static characteristics of main steam regulating valves. Failure to distinguish them may lead to biased estimates of the nonlinear static characteristics of main steam regulating valves.

Industrial big data is collected from the daily operation process and contains rich modeling information, which can be extracted through data mining technology for model identification [23], [24]. Data segments in steady states are often used in the literature to identify nonlinear models [25], [26]. However, steady-state segments may only cover some isolated ranges of the nonlinear flow characteristics, making it difficult to describe changes in nonlinear flow characteristics over a large range. The input signal of thermal power generation units is generally not a step signal with large amplitude changes, but multiple slope signals changing in a trapezoidal manner.

The main contribution of the article is to identify nonlinear flow characteristics of main steam regulating valves based on slope-response segments and steady-state segments, referred to as special segments, hidden in historical operating data. To the best of our knowledge, slope-response segments have not been exploited for the identification of nonlinear models by existing methods in the literature. Relationships between a nonlinear model of flow characteristics and the special segments are theoretically established, to prove that the nonlinear model of flow characteristics is isolated from the dynamics of steam turbines and generators. The nonlinear model parameters are estimated by solving an optimization problem via a linear dynamic programming algorithm. The validity of the identified nonlinear model can be visually verified by comparing measured outputs in special segments with simulated model outputs.

The novelty of the proposed method is to exploit these special segments in order to separate the nonlinear model of flow characteristics from the dynamics of steam turbines and generators. Such a separation is highly necessary, to be demonstrated by a comparison with existing methods via industrial case studies and simulation investigations (given later in Section IV). The Hammerstein model identification method and the sparse identification method use all measured data to simultaneously identify nonlinear static and dynamic models. However, dynamic characteristics change significantly at different operating points, making it difficult to accurately estimate nonlinear static characteristics. For the proposed method, the special segments only contain nonlinear static information reflecting the flow characteristics of main steam regulating valves, so that they are not affected by the changes in dynamic characteristics.

The rest of this article is organized as follows. Section II describes the problem to be solved. Section III gives detailed steps of the proposed method. Section IV provides industrial cases for illustration. Finally, Section V concludes this article.

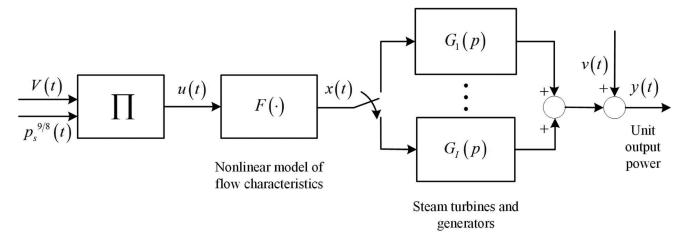


Fig. 1. Steam turbine power control system.

II. PROBLEM DESCRIPTION

Consider a steam turbine power control system depicted in Fig. 1, where V is the control valve opening, p_s is the main steam pressure, and y is the generated power output. Under a condition that the main steam temperature is unchanged, a boiler-turbine model in steady states is [27]

$$y = \alpha_1 \left(V \cdot p_s^{9/8} - \alpha_2 \right) \quad (1)$$

where α_1 is the coefficient associated with the boiler-turbine system and α_2 is the coefficient of the initial state of the steam. In Fig. 1, $u = V \cdot p_s^{9/8}$ is defined as the integrated control valve input owing to (1).

The flow characteristics of regulating valves are modeled as a nonlinear model $F(\cdot)$, taking u as the input and x as the unmeasurable output. The nonlinear model $F(\cdot)$ can be approximated by several interconnected line segments to form a piecewise linear function as

$$x(t) = F(u(t)) = K_{f,j}u(t) + C_j, \text{ for } u_j \leq u(t) \leq u_{j+1}. \quad (2)$$

Here, $K_{f,j}$ and C_j are the slope and intercept of the j th segment for $j = 1, 2, \dots, J$, where J is the number of piecewise functions. The boundary point vector of $F(\cdot)$ is denoted as $\mathbf{U} = [u_1, \dots, u_j, \dots, u_{J+1}]$. Such a piecewise linear function is widely adopted because its inverse function is readily available in order to compensate for nonlinear flow characteristics.

The dynamics of steam turbines and generators usually vary at different operating points (see industrial data samples in Fig. 10 at Section IV later). Hence, the dynamics of steam turbines and generators are described by multiple dynamic models G_1, \dots, G_I rather than a single one. Due to Taylor expansions, G_i around the i th operating point can be approximated by a first-order linear time-invariant model in the Laplace domain [28], i.e.,

$$G_i(s) = \frac{K_{g,i}e^{-\tau_i s}}{T_i s + 1} \quad (3)$$

where $K_{g,i}$, T_i , and τ_i are the static gain, time constant, and time delay of G_i for $i = 1, 2, \dots, I$, respectively. By introducing $t \in \mathbb{R}$ as a real-valued time index and $p = d/dt$ as the differentiation operator, the generated power output $y(t)$ is obtained as

$$y(t) = x(t)G_i(p) + v(t) = y_o(t) + v(t) \quad (4)$$

where

$$y_o(t) = \frac{K_{g,i}x(t - \tau_i)}{T_i p + 1}, \text{ for } x_i \leq x(t) < x_{i+1}. \quad (5)$$

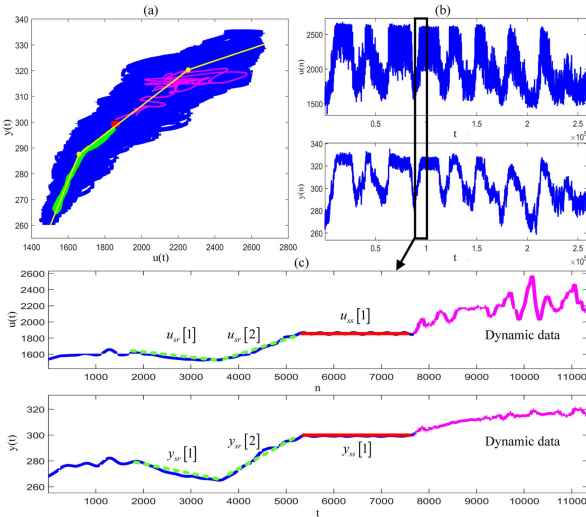


Fig. 2. Schematic diagram to illustrate the separation and identification of nonlinear flow characteristics for the proposed method.

Here, $v(t)$ represents some unmeasurable noise and $y_o(t)$ is the noise-free counterpart of $y(t)$. The symbol x_i is the boundary point of $x(t)$ corresponding to G_i , which is formulated as the vector $\mathbf{X} = [x_1, \dots, x_i, \dots, x_{I+1}]$. There is a gain ambiguity between the nonlinear function $F(\cdot)$ and the dynamic linear model G_i . A standard solution is to remove the gain ambiguity between $K_{g,i}$ and $K_{f,j}$ by setting $K_{g,i} = 1$ [16].

Given historical data samples $\{u(n), y(n)\}_{n=1}^N$, our objective is to estimate parameters $K_{f,j}$'s and C_j 's of the nonlinear model $F(\cdot)$ in (2). Here, $n \in \mathbb{Z}^+$ is the sampling index associated with the sampling period h , N is the total data length, and \mathbb{Z}^+ is the set of positive integers. The estimated nonlinear model $\hat{F}(\cdot)$ represents the flow characteristics of main steam regulating valves. The dynamic model parameters T_i and τ_i are not estimated in the article; even so, the accuracy of the estimated nonlinear model $\hat{F}(\cdot)$ can be verified by comparing $y(t)$ with $\hat{y}(t)$ as the estimate of $x(t)$ in the special segments where dynamics of G_i 's are absent.

III. PROPOSED METHOD

This section first presents the main idea of the proposed method. Second, relationships between special segments and a nonlinear model of flow characteristics are theoretically established. Finally, the nonlinear model is identified by a dynamic programming algorithm.

A. Main Idea of the Proposed Method

Due to a fact that steam turbines and generators have different dynamic characteristics at different operating points, the static nonlinear flow characteristics are overwhelmed by input and output data with dynamic characteristics, such as the blue dots in Fig. 2(a) and their corresponding time series are shown in Fig. 2(b). In other words, the true nonlinear flow characteristics [e.g., yellow solid line in Fig. 2(a)] is difficult to identify accurately under the influence of some dynamic data [e.g., magenta solid line in Fig. 2(a)]. The key to identifying the nonlinear flow

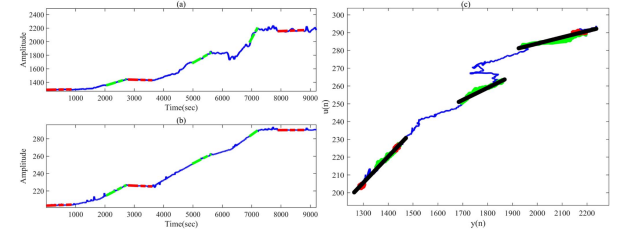


Fig. 3. Some industrial data samples: (a) $u(t)$ (blue solid), steady-state segments $\hat{u}_{ss}[m]$ with $m = 1, 2, 3$ (red dash) and slope-response segments $\hat{u}_{sr}[l]$ with $l = 1, 2, 3$ (green dash); (b) $y(t)$ (blue solid), $\hat{y}_{ss}[m]$ (red dash), and $\hat{y}_{sr}[l]$ (green dash); (c) scatter plot of $u(t)$ and $y(t)$ (blue dot), scatter of $\hat{u}_{ss}[m]$ and $\hat{y}_{ss}[m]$ (red dot), scatter of $\hat{u}_{sr}[l]$ and $\hat{y}_{sr}[l]$ (green dot), and the simulated outputs obtained from special segments (black solid).

characteristics is to separate it from the linear dynamic submodels at different operating points. The separation is achieved based on some special segments. One type of special segments is referred to as the steady-state segments with constant amplitudes, denoted as $u_{ss}[m]$ and $y_{ss}[m]$ for $m = 1, 2, \dots$ [e.g., red solid lines in Fig. 2(c)], where the lowercase ss is the abbreviation for steady-state. The other type of special segments is taken as the slope-response segments with large amplitude changes, denoted as $u_{sr}[l]$ and $y_{sr}[l]$ for $l = 1, 2, \dots$ [e.g., green dash lines in Fig. 2(c)], where the lowercase sr is the abbreviation for slope response.

The special segments are proven later in Proposition 1 to be absent of dynamic information, so that they can be used to identify the nonlinear model $F(\cdot)$ in (2). In particular, the identification of $F(\cdot)$ is formulated as an optimization problem. Taking Fig. 2(a) as an example, the nonlinear flow characteristics are optimally described by three piecewise basis functions in (2). The slope $K_{f,j}$ and intercept C_j of the j th segment are estimated after the boundary point vector $\mathbf{U} = [u_1, \dots, u_{J+1}]$ is determined.

Let us look at some industrial data samples to justify the existence of nonlinear flow characteristics. The input $u(t)$ and output $y(t)$ rise from one steady state to another in Fig. 3(a), (b). However, the changes in $u(t)$ and $y(t)$ are in a nonlinear relationship, as evidenced by the black solid lines in Fig. 3(c). The black solid lines are the simulated outputs obtained by fitting special segments at different positions. The rising slopes of the black lines are obviously different, indicating that the flow characteristics of main steam regulating valves are indeed nonlinear.

B. Relationships Establishment Between Special Segments and a Nonlinear Model

First, the steady-state segments and slope-response segments $\{y_{ss}[m], u_{ss}[m]\}_{m=1}^M$ and $\{y_{sr}[l], u_{sr}[l]\}_{l=1}^L$ are extracted from $\{u(n), y(n)\}_{n=1}^N$ by applying piecewise linear representation (PLR) technology [29]. Here, M and L are the numbers of the steady-state segments and slope-response segments. The main idea is to represent the changing trend of long time sequences by several short straight lines, and find the lines with small and large amplitude changes as the steady-state and slope-response

segments, respectively. The detailed steps for extracting special segments can be found in literatures [26], [30]. Data segments of $u(n)$ and $y(n)$ of the m th steady-state segment are represented as

$$u_{ss}[m] = \{u(n)\}_{n=n_{m,s}}^{n_{m,e}}, y_{ss}[m] = \{y(n)\}_{n=n_{m,s}}^{n_{m,e}} \quad (6)$$

where $n_{m,s}$ and $n_{m,e}$ are the starting index and ending index of the m -th steady-state segment, respectively. Similarly, data segments of $u(n)$ and $y(n)$ of the l -th slope-response segment are represented as

$$u_{sr}[l] = \{u(n)\}_{n=n_{l,s}}^{n_{l,e}}, y_{sr}[l] = \{y(n)\}_{n=n_{l,s}}^{n_{l,e}} \quad (7)$$

where $n_{l,s}$ and $n_{l,e}$ are the starting index and ending index of the l -th slope-response segment, respectively.

Second, Proposition 1 gives the mathematical relationships between the special segments and the nonlinear model $F(\cdot)$.

Proposition 1: Under the condition that the number J of piecewise functions is known, the steady-state segments ($y_{ss}[m], u_{ss}[m]$) and the slope-response segments ($y_{sr}[l], u_{sr}[l]$) are respectively related to the slope $K_{f,j}$ and intercept C_j of the nonlinear model $F(\cdot)$ in (2) as

$$y_{ss}[m] = K_{f,j}u_{ss}[m] + C_j, \text{ for } u_j \leq u_{ss}[m] < u_{j+1}, \quad (8)$$

$$y_{sr}[l] = K_{f,j}u_{sr}[l] + C_j, \text{ for } u_j \leq u_{sr}[l] < u_{j+1}. \quad (9)$$

Here, u_j and u_{j+1} are the boundary points of $u(t)$ in (2) with $j = 1, \dots, J$.

Proof: The input $u(t)$ of the nonlinear model of flow characteristics in a slope response can be described as

$$u(t) = \eta_1 t + \eta_2 \quad (10)$$

where η_1 and η_2 are the slope and intercept parameters, respectively. The unmeasured $x(t)$ is obtained by

$$x(t) = F(u(t)) = K_{f,j}(\eta_1 t + \eta_2) + C_j, \text{ for } u_j \leq u(t) \leq u_{j+1}. \quad (11)$$

The Laplace transform of the generated power output $y(t)$ of $G_i(s)$ in (3) subject to $u(t)$ is

$$\begin{aligned} y(s) &= G_i(s)X(s) \\ &= \frac{e^{-\tau_i s}}{T_i s + 1} \cdot \left(\frac{K_{f,j}\eta_1}{s^2} + \frac{K_{f,j}\eta_2 + C_j}{s} \right) \\ &= \left(\frac{K_{f,j}\eta_1}{s^2} - \frac{T_i K_{f,j}\eta_1}{s} + \frac{T_i K_{f,j}\eta_1}{s + 1/T_i} \right. \\ &\quad \left. + \frac{K_{f,j}\eta_2 + C_j}{s} - \frac{K_{f,j}\eta_2 + C_j}{s + 1/T_i} \right) e^{-\tau_i s}. \end{aligned} \quad (12)$$

The time-domain expression of $y(t)$ is

$$\begin{aligned} y(t) &= K_{f,j}\eta_1(t - \tau_i) - T_i K_{f,j}\eta_1 \left(1 - e^{-\frac{t-\tau_i}{T_i}} \right) \\ &\quad + (K_{f,j}\eta_2 + C_j) \left(1 - e^{-\frac{t-\tau_i}{T_i}} \right) \end{aligned} \quad (13)$$

where the term $e^{-((t-\tau_i)/T_i)}$ decreases rapidly as t increases, and tends to zero after $t \geq (5T_i + \tau_i)$, as shown in Table I. Thus, when t is large, $y(t)$ reaches a steady state and can be

TABLE I
TYPICAL VALUES OF $e^{-((t-\tau_i)/T_i)}$

$t - \tau_i$	T_i	$2T_i$	$3T_i$	$4T_i$	$5T_i$	$6T_i$
$e^{-((t-\tau_i)/T_i)}$	0.3679	0.1353	0.0498	0.0183	0.0067	0.0025

approximated as

$$\begin{aligned} y(t) &\approx K_{f,j}\eta_1(t - \tau_i) - T_i K_{f,j}\eta_1 + K_{f,j}\eta_2 + C_j \\ &= K_{f,j}(\eta_1 t + \eta_2 - \eta_1(T_i + \tau_i)) + C_j \\ &= K_{f,j}u(t - T_i - \tau_i) + C_j \\ &\approx K_{f,j}u(t) + C_j. \end{aligned} \quad (14)$$

Here, $K_{f,j}$ and C_j are, respectively, the slope and intercept of the j th segment with $j = 1, 2, \dots, J$, and the boundary point vector of $u(t)$ is $\mathbf{U} = [u_1, \dots, u_{J+1}]$. The time constant T_i of the steam turbine power control system is small compared to the time duration of slope responses, so that the condition $t \geq (5T_i + \tau_i)$ can usually be satisfied. For instance, as shown in Figs. 2(c) and 3(a), (b), $y(t)$ follows $u(t)$ in straight lines at slope responses.

Given the segments $u_{sr}[l]$ and $y_{sr}[l]$ in the slope response with large amplitude changes, as shown by the green dash lines in Figs. 2(b) and 3(a), (b), (14) becomes

$$y_{sr}[l] = K_{f,j}u_{sr}[l] + C_j, \text{ for } u_j \leq u_{sr}[l] < u_{j+1}. \quad (15)$$

Given the segments $u_{ss}[m]$ and $y_{ss}[m]$ in steady-state conditions with constant amplitudes, as shown by the red dash lines in Figs. 2(b) and 3(a), (b), (14) becomes

$$y_{ss}[m] = K_{f,j}u_{ss}[m] + C_j, \text{ for } u_j \leq u_{ss}[m] < u_{j+1} \quad (16)$$

where C_j is a nonzero constant between $u_{ss}[m]$ and $y_{ss}[m]$.

Hence, (8) and (9) are proven. \square

C. Identification of the Nonlinear Model of Flow Characteristics

Data samples of the special segments are embedded into two sets

$$\begin{aligned} \Psi_u &= \{u_{ss}[1], \dots, u_{ss}[M], u_{sr}[1], \dots, u_{sr}[L]\} \\ &= \{\varphi_u(1), \dots, \varphi_u(N_s), \varphi_u(N_s + 1), \dots, \varphi_u(N_s + N_c)\}, \\ \Psi_y &= \{y_{ss}[1], \dots, y_{ss}[M], y_{sr}[1], \dots, y_{sr}[L]\} \\ &= \{\varphi_y(1), \dots, \varphi_y(N_s), \varphi_y(N_s + 1), \dots, \varphi_y(N_s + N_c)\}. \end{aligned} \quad (17)$$

Here, N_s and N_c are the number of data samples for M steady-state segments with constant amplitudes and L slope-response segments with large amplitude changes, respectively. The length of Ψ_u and Ψ_y is denoted as $N_E = N_s + N_c$. Sorting Ψ_u in the ascending order yields a set Ψ_{us} as

$$\Psi_{us} = \{\psi_u(1), \dots, \psi_u(\varepsilon), \dots, \psi_u(N_E)\} \quad (18)$$

satisfying

$$\psi_u(1) < \dots < \psi_u(\varepsilon) < \psi_u(\varepsilon + 1) \dots < \psi_u(N_E).$$

Data samples in Ψ_y are rearranged according to the sorting order of Ψ_{us} to form a new set $\Psi_{ys} = \{\psi_y(1), \dots, \psi_y(\varepsilon), \dots, \psi_y(N_E)\}$.

The nonlinear model $F(\cdot)$ of flow characteristics can be identified by the special segment sets Ψ_{us} and Ψ_{ys} . An optimization problem is formulated to simultaneously determine the number J of piecewise functions and the boundary point vector \mathbf{U} , i.e.,

$$\Omega(J) = \min_{\substack{u_1, \dots, u_{j+1}, \\ K_{f,1}, \dots, K_{f,J}, C_1, \dots, C_J}} \sum_{j=1}^J (\Psi_{ys,j} - \hat{\Psi}_{ys,j})^2 \quad (19)$$

where $\Psi_{ys,j}$ denotes the data samples of j th segment in Ψ_{ys} , and $\hat{\Psi}_{ys,j} = \hat{K}_{f,j}\Psi_{us,j} + \hat{C}_j$ is the estimate of $\Psi_{ys,j}$ for $j = 1, \dots, J$. The estimates of slope and intercept parameters $\hat{K}_{f,j}$'s and \hat{C}_j 's are obtained from multiple linear equations via the least squares algorithm based on $\Psi_{ys,j}$ and $\Psi_{us,j}$, i.e.,

$$\hat{\theta}_j = (\Phi_{us}^T \Phi_{us})^{-1} \Phi_{us}^T \Phi_{ys} \quad (20)$$

where

$$\theta_j = \begin{bmatrix} C_j \\ K_{f,j} \end{bmatrix}, \Phi_{ys} = \begin{bmatrix} \Psi_{ys,j}(1) \\ \Psi_{ys,j}(2) \\ \vdots \\ \Psi_{ys,j}(N_{E,j}) \end{bmatrix},$$

$$\Phi_{us} = \begin{bmatrix} 1 & \Psi_{us,j}(1) \\ 1 & \Psi_{us,j}(2) \\ \vdots & \vdots \\ 1 & \Psi_{us,j}(N_{E,j}) \end{bmatrix}.$$

Here, $N_{E,j}$ is the length of data samples in $\Psi_{ys,j}$ and $\Psi_{us,j}$.

An efficient linear dynamic programming algorithm [31] is used to solve the optimization problem in (19). The predefined range of the piecewise number $R_p = [1, R_{\max}]$ is set based on the nonlinear characteristics of regulating valves. Define $\Omega_{j,r}$ as the minimum cost of fitting the data samples $\Psi_{ys}(1:r)$ by j piecewise functions with $j = 1, 2, \dots, J$, and the ending point of j th piecewise function being at the position index $a_{j+1} = r$. All position indices of J piecewise functions are embedded as a vector $\mathbf{A} = [a_1, \dots, a_{J+1}]$. The schematic illustration of the linear dynamic programming algorithm is shown in Fig. 4, and the following iterative substeps are performed to determine the position index vector \mathbf{A} for J piecewise functions.

1) Initialize the minimal cost $\Omega_{1,r}$, i.e.,

$$\Omega_{1,r} = \min \|\Psi_{ys,1} - \hat{\Psi}_{ys,1}\|^2, \text{ for } 1 < r \leq N_E - J + 1,$$

$$\text{s.t. } \Psi_{ys,1} = \Psi_{ys}(a_1 : a_2), a_1 = 1, a_2 = r. \quad (21)$$

Here, the mathematical symbol $\|\cdot\|$ represents the L-2 norm.

2) Minimize the cost $\Omega_{j,r}$ by searching for possible starting points of piecewise functions from 2 to $J-1$ when $\Omega_{j-1,r}$ becomes available, i.e.,

$$\Omega_{j,r} = \min_{j \leq w < r} [\Omega_{j-1,w} + \|\Psi_{ys,j} - \hat{\Psi}_{ys,j}\|^2],$$

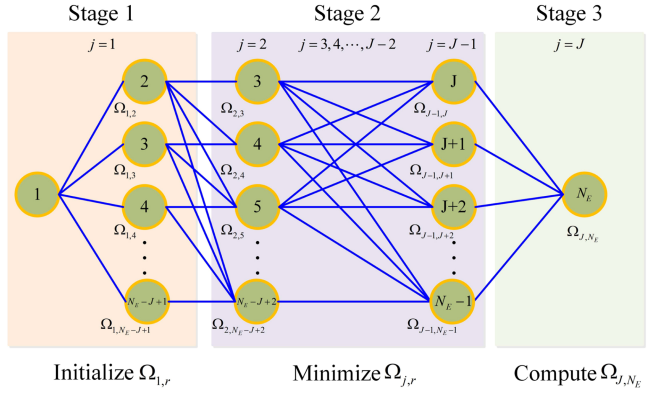


Fig. 4. Schematic illustration of the linear dynamic programming algorithm.

for $1 < j \leq J-1, j < r \leq N_E - J + j$,

$$Z_{j-1,r} = \arg \min_{j \leq w < r} [\Omega_{j-1,w} + \|\Psi_{ys,j} - \hat{\Psi}_{ys,j}\|^2],$$

$$\text{s.t. } \Psi_{ys,j} = \Psi_{ys}(a_j : a_{j+1}), a_j = w, a_{j+1} = r. \quad (22)$$

3) Compute the minimal cost Ω_{J,N_E} because the position index for the ending point of J th piecewise function is equal to the length of data samples in Ψ_{ys} , i.e.,

$$\Omega_{J,N_E} = \min_{J \leq w < N_E} [\Omega_{J-1,w} + \|\Psi_{ys,J} - \hat{\Psi}_{ys,J}\|^2],$$

$$Z_{J-1,N_E} = \arg \min_{J \leq w < N_E} [\Omega_{J-1,w} + \|\Psi_{ys,J} - \hat{\Psi}_{ys,J}\|^2],$$

$$\text{s.t. } \Psi_{ys,J} = \Psi_{ys}(a_J : a_{J+1}), a_J = w, a_{J+1} = N_E. \quad (23)$$

The position matrix Z is used to record the optimal position indices of j piecewise functions in (22) and (23), where $j = 1, 2, \dots, J$. The values $\Omega(J)$ with $J \in R_p$ are obtained by performing the above iterative steps R_{\max} times.

Being inspired by an idea in [32], the optimal number of piecewise functions is determined by

$$J^* = \operatorname{argmax} \Lambda(J) = \operatorname{argmax} \frac{\log \left(\frac{\Omega(J-1)}{\Omega(J)} \right) - \log \left(\frac{\Omega(J)}{\Omega(J+1)} \right)}{\log \left(\frac{\Omega(J-1)}{\Omega(J)} \right) + \log \left(\frac{\Omega(J)}{\Omega(J+1)} \right)}. \quad (24)$$

Equation (24) has a clear physical meaning. As J in (2) increases, a curve of J and the logarithm function $\log(\Omega(J))$ of (19) is formed [see, e.g., Fig. 6(a) given later in Section IV]. The point $(J^*, \log(\Omega(J^*)))$ on the curve is considered as the inflection point with a maximum turning angle between η_1 and η_2 , where η_1 and η_2 represent the lines between $\log(\Omega(J^*-1))$, $\log(\Omega(J^*))$, and $\log(\Omega(J^*+1))$, respectively. Taking Fig. 6(a) as an example, there is a maximum turning angle from $\eta_1 = \log(\Omega(3)) - \log(\Omega(4))$ to $\eta_2 = \log(\Omega(4)) - \log(\Omega(5))$, which means that the decreasing speed of η_1 is fast, and then slows down in η_2 . Therefore, the value $J^* = 4$ at the inflection point is selected as the optimal number of piecewise functions, which

has a relatively small cost function and effectively avoids the risk of overfitting.

The position index vector $A_{J^*} = \{a_1, \dots, a_{J^*+1}\}$ is obtained sequentially by executing the trace-back procedure after determining the optimal number J^* of piecewise functions by (24). The estimates of the boundary point vector \mathbf{U} are determined according to A_{J^*} as $\hat{\mathbf{U}} = [\hat{u}_1, \dots, \hat{u}_j, \dots, \hat{u}_{J^*+1}]$, where $\hat{u}_j = \Psi_{us}(a_j)$.

The time complexity and space complexity of using dynamic programming algorithm are analyzed as follows. When $J \geq 2$, the total number of times to execute the substeps 1)–3) in (21)–(23) is

$$\Gamma = \frac{J-2}{2}N_E^2 + \left(4 - \frac{J^2}{2}\right)N_E + \frac{J^3}{6} + \frac{5}{6}J - 2 \quad (25)$$

where N_E is the length of data samples in Ψ_{ys} . The time complexity is measured by the execution number of the algorithm in (25), expressed in Big O notation [33], namely $O(N_E^2)$. The space occupied by performing calculations is linearly related to N_E , so that the space complexity is $O(N_E)$. Taking the industrial case appeared later in Section IV, for instance, the dynamic programming algorithm takes about 18 minutes to solve the optimal problem in (19) on a personal computer with an Intel i7 3.4-GHz CPU and 16-GB memory, where $J = 4$ and $N_E = 305633$ (equivalent to 84.9 h of data samples with the sampling period $h = 1$ s). It is completely acceptable for offline identification of nonlinear models.

Finally, the nonlinear model $F(\cdot)$ in (2) is represented by the estimates $\hat{\theta}_j$'s in (20) as

$$\hat{x}(t) = \hat{F}(u(t)) = \hat{K}_{f,j}u(t) + \hat{C}_j, \text{ for } \hat{u}_j \leq u(t) \leq \hat{u}_{j+1}. \quad (26)$$

The unbiased analysis of the estimated parameter vector $\hat{\theta}_j$ of the nonlinear model $F(\cdot)$ is given by Proposition 2.

Proposition 2: Under the conditions that the random error ϵ is with zero mean, and the length N_E of special data samples $\{\Psi_{us}, \Psi_{ys}\}$ goes to infinity, $\hat{\theta}_j$ in (20) is the unbiased estimate of the true parameter vector θ_j of $F(\cdot)$ with $j = 1, \dots, J^*$, i.e., $E(\hat{\theta}_j) = \theta_j$.

Proof: According to Proposition 1, the measurements of the special segment sets Ψ_{ys} and Ψ_{us} obey the linear regression model

$$\mathbf{Y} = \mathbf{U}\theta_j + \epsilon$$

where $\mathbf{Y} = [y(1), \dots, y(N_{E,j})]^T$, $\mathbf{U} = \begin{bmatrix} \mathbf{I} \\ \mathbf{U}_j \end{bmatrix}^T = \begin{bmatrix} 1 & \dots & 1 \\ u(1) & \dots & u(N_{E,j}) \end{bmatrix}^T$, and $\epsilon = [\varepsilon(1), \dots, \varepsilon(N_{E,j})]^T$. $N_{E,j}$ is the length of data samples in $[\hat{u}_j, \hat{u}_{j+1}]$ with $j = 1, \dots, J^*$, and $N_E = \sum_{j=1}^{J^*} N_{E,j}$ is the length of data samples in Ψ_{us} .

From the properties of the dynamic programming algorithm, it can be known that the solution satisfying the optimization function in (19) is optimal, and any part of the solution is also optimal for the subproblem [34]. The optimal estimate of the boundary point vector $\hat{\mathbf{U}}$ for $\Omega(J^*)$ tends to the true vector \mathbf{U} when $N_E \rightarrow \infty$. Therefore, for the subproblem in (20), the least squares estimate of $\hat{\theta}_j$ corresponding to $\Psi_{us} \in [\hat{u}_j, \hat{u}_{j+1}] \rightarrow$

$[u_j, u_{j+1}]$ is

$$\begin{aligned} \hat{\theta}_j &= (\Phi_{us}^T \Phi_{us})^{-1} \Phi_{us}^T \Phi_{ys} \\ &= (\Phi_{us}^T \Phi_{us})^{-1} \Phi_{us}^T (\Phi_{us} \theta_j + \epsilon) \\ &= (\Phi_{us}^T \Phi_{us})^{-1} \Phi_{us}^T \Phi_{us} \theta_j + (\Phi_{us}^T \Phi_{us})^{-1} \Phi_{us}^T \epsilon \\ &= \theta_j + (\Phi_{us}^T \Phi_{us})^{-1} \Phi_{us}^T \epsilon. \end{aligned} \quad (27)$$

Calculating the expectation on both sides of (27) gives

$$E(\hat{\theta}_j) = E(\theta_j) + (\Phi_{us}^T \Phi_{us})^{-1} \Phi_{us}^T E(\epsilon). \quad (28)$$

From the condition $E(\epsilon) = 0$, (28) becomes

$$E(\hat{\theta}_j) = E(\theta_j). \quad (29)$$

Therefore, $\hat{\theta}_j$ is an unbiased estimator of θ_j for $j = 1, \dots, J^*$ based on the Gauss Markov theorem [35]. \square

The identifiability of the proposed method is discussed to support Proposition 2. The relationship between $y_{ss}[m]$ and $u_{ss}[m]$ (as well as $y_{sr}[l]$ and $u_{sr}[l]$) can be linearly represented by the parameters $K_{f,j}$ and C_j according to Proposition 1. In the piecewise interval $[u_j, u_{j+1}]$ of $u(t)$, if there are at least two linearly independent special segments $\{u_{ss}[m], y_{ss}[m]\}$ and $\{u_{sr}[l], y_{sr}[l]\}$, the parameters $K_{f,j}$ and C_j in (2) can be uniquely determined. This condition can be easily satisfied since a large number of special segments are extracted from historical data. In other words, when the matrix Φ_{us} has a full-column rank, the vector $\hat{\theta}_j = [\hat{K}_{f,j}, \hat{C}_j]$ can be uniquely determined by (20) based on the data samples in $\Psi_{us,j}$ and $\Psi_{ys,j}$. Note that $\Psi_{us,j}$ consists of $u_{ss}[m]$ and $u_{sr}[l]$ within the estimated piecewise interval $[\hat{u}_j, \hat{u}_{j+1}]$, and $\Psi_{ys,j}$ consists of the corresponding $y_{ss}[m]$ and $y_{sr}[l]$. Therefore, when the length of Φ_{us} goes to infinity, $\hat{\theta}_j$ approaches the true parameter vector θ_j so that the nonlinearity $F(\cdot)$ is said to be identifiable [36].

IV. INDUSTRIAL CASE STUDIES

This section provides industrial case studies to illustrate the proposed method and compare it with the Hammerstein identification method and the sparse identification method.

A steam turbine control system of a 300-MW coal-fired power generation unit is investigated. It takes the same control diagram as that in Fig. 1. Data samples of the generated power output y in MW, the control valve opening V in %, the valve inlet pressure p_s in MPa, and the main steam temperature T in °C are collected with the sampling period $h = 1$ s. The integrated control valve input $u = V \cdot p_s^{9/8}$ is formulated as the input to the nonlinear model of flow characteristics.

The proposed method is applied to ten days of data samples. In Fig. 5(a), the main steam temperature fluctuates no more than 1°C around the average value 539 °C when the input $u(t)$ and output $y(t)$ change greatly. It is observed that the main steam temperature is usually in a relatively stable state in practice, so that the condition in (1) with an unchanged main steam temperature is satisfied. Fig. 5(b), (c) shows part of the data samples used for nonlinear model identification at different power values. First, the steady-state segments $\{y_{ss}[m], u_{ss}[m]\}_{m=1}^{116}$ with constant amplitudes and the slope-response segments

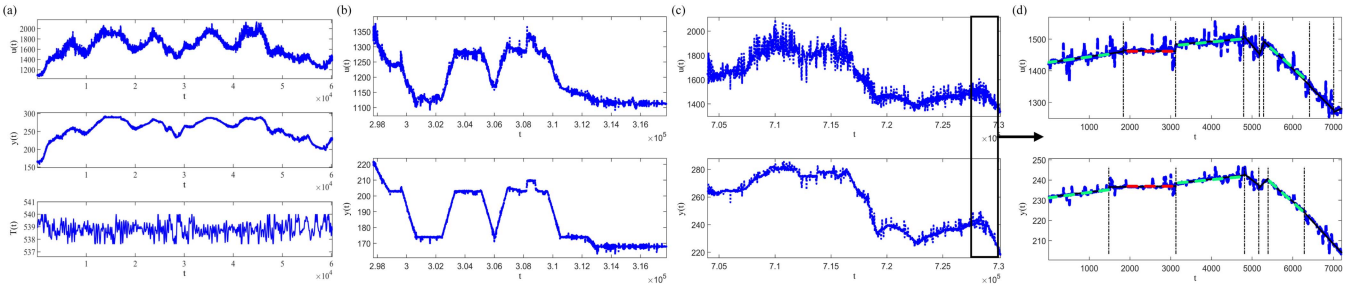


Fig. 5. Partial data samples for nonlinear model identification at different power values: (a) $u(t)$ (blue dot) at the top, $y(t)$ (blue dot) in the middle, and $T(t)$ (blue dot) at the bottom, (b) and (c): $u(t)$ (blue dot) at the top, $y(t)$ (blue dot) at the bottom, and the PLR of $\{u(n)\}_{n=1}^{3600}$ at the top in (d); $u(t)$ (blue solid), $\hat{u}_d(t)$ (black solid), $u_{ss}[1]$ (red dash), $u_{sr}[l]$ with $l = 1, 2, 3$ (green dash), the counterparts of $\{y(n)\}_{n=1}^{3600}$ at the bottom.

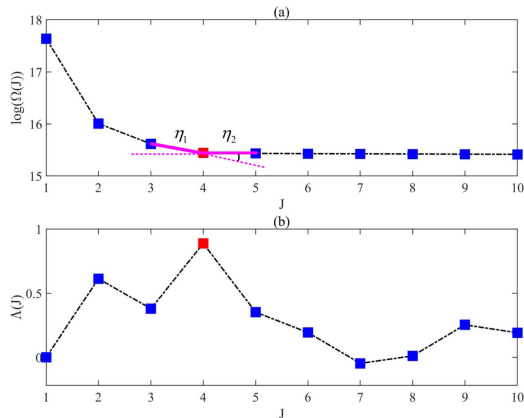


Fig. 6. Determine the optimal number of piecewise functions: (a) the curve of J and $\log(\Omega(J))$ with $J = 1, \dots, 10$, (b) the calculated values $\Lambda(J)$ in (24).

$\{y_{sr}[l], u_{sr}[l]\}_{l=1}^{460}$ with large amplitudes are respectively obtained from $\{u(n), y(n)\}_{n=1}^N$ with $N = 864000$. The PLR result of two-hour data samples is shown in Fig. 5(d), where the special segments $\{u_{ss}[1], y_{ss}[1]\}$ and $\{u_{sr}[l], y_{sr}[l]\}_{l=1}^3$ are marked with red and green dash lines, respectively. These special segments are embedded in the sets Ψ_u and Ψ_y in (17). The set Ψ_u is sorted as Ψ_{us} in (18), and Ψ_{ys} is obtained according to the sorting order of Ψ_{us} , where the length of the data samples in Ψ_{us} is $N_E = 305633$. Second, the optimal number $J^* = 4$ of piecewise functions is determined by (24). Fig. 6(a) shows the curve of J and $\log(\Omega(J))$ with $J = 1, \dots, 10$, and the calculated values $\Lambda(J)$ in (24) are given in Fig. 6(b). Simultaneously, the piecewise interval of $u(t)$ corresponding to the boundary point vector \mathbf{U} , and the estimates of slopes and intercepts $K_{f,j}$'s and C_j 's are obtained by (19)–(23), respectively, as listed in Table II. The estimated nonlinear model $\hat{F}(u(t))$ of flow characteristics is obtained by (2) as

$$\hat{F}(u(t)) = \begin{cases} 0.2181 \cdot u(t) - 75.932, & 1082.19 \leq u(t) < 1255.28 \\ 0.1802 \cdot u(t) - 28.2311, & 1255.28 \leq u(t) < 1609.07 \\ 0.0862 \cdot u(t) + 123.0493, & 1609.07 \leq u(t) < 1875.42 \\ 0.0157 \cdot u(t) + 255.2569, & 1875.42 \leq u(t) < 2336.11 \end{cases} \quad (30)$$

TABLE II
IDENTIFICATION RESULTS OF THE PROPOSED METHOD AND THE HAMMERSTEIN IDENTIFICATION METHOD

Method	j	$\hat{K}_{f,j}$	\hat{C}_j	$[\hat{u}_j, \hat{u}_{j+1}]$
The proposed method	1	0.2181	-75.932	[1082.19, 1255.28]
	2	0.1802	-28.2311	[1255.28, 1609.07]
	3	0.0862	123.0493	[1609.07, 1875.42]
	4	0.0157	255.2569	[1875.42, 2336.11]
The Hammerstein identification method	1	0.2261	-86.696	[1079.48, 1312.49]
	2	0.1659	-7.6326	[1312.49, 1571.59]
	3	0.0823	123.6836	[1571.59, 1916.49]
	4	0.0147	253.1876	[1916.49, 2352.17]

As a comparison, the Hammerstein identification method and the sparse identification method are deployed for the same data samples. For the Hammerstein identification method, the function “nlhw” in MATLAB System Identification Toolbox [37] is used to simultaneously identify the nonlinear model and the single dynamic linear submodel. The piecewise interval of $u(t)$ and the estimates of $K_{f,j}$'s and C_j 's from the Hammerstein identification method are listed in Table II. The deficiency of the proposed method is that the maximum value of $u(t)$ for special segments is 2336.11 in Table II, less than 2352.17 of the Hammerstein identification method based on all historical data. However, the deficiency is acceptable since there are no special segments in historical data to tell the information about the unknown nonlinear model $F(\cdot)$ for $u(t)$ larger than 2336.11. The estimated nonlinear model from the Hammerstein identification method may be inaccurate, as illustrated later in Fig. 9 and Table III.

For the sparse identification method, the library of candidate nonlinear functions is selected as $\Theta(\mathbf{W}) = [\mathbf{W} \mathbf{W}^P_2 \mathbf{W}^P_3 \sin(\mathbf{W}) \cos(\mathbf{W})]$, where $\mathbf{W} = [\mathbf{Y} \mathbf{U}]_{N \times 2}$ is the matrix of data samples of $y(t)$ and $u(t)$, and N is the length of the data sample for identification. \mathbf{W}^P_2 and \mathbf{W}^P_3 are higher polynomial matrices, e.g., $\mathbf{W}^P_2 = [\mathbf{Y}^2 \mathbf{Y} \times \mathbf{U} \mathbf{U}^2]$. The sparse regression problem is formulated as $\hat{\mathbf{Y}} = \Theta(\mathbf{W})\Xi$, where $\hat{\mathbf{Y}}_{N \times 1}$ is the derivative matrix of $y(t)$, and $\Xi = [\xi_1, \dots, \xi_{14}]$ is the sparse vector of coefficients. The sparse vector is estimated by the method in [13], i.e., $\hat{\Xi} = [-95.05, -0.47, 0.26, 0, -5.75 \times 10^{-5}, -7.56 \times 10^{-6}, 1.29 \times 10^{-4}, -3.86 \times 10^{-6}, 0, -2.01 \times 10^{-8}, -1.01, 0, -1.08, 0]$. Fig. 7 shows the ten days data samples of $u(t)$ and $y(t)$ as the grey dots. It can be observed that

TABLE III
MEAN SQUARE ERRORS OF THE THREE METHODS FOR THE SPECIAL SEGMENTS

Special segments	The proposed method	The Hammerstein identification method	The sparse identification method
$y_{ss}[1]$	18.971	8.41×10^3	3.39×10^3
$y_{ss}[2]$	195.94	8.64×10^4	5.71×10^3
$y_{ss}[3]$	121.07	4.71×10^4	8.01×10^4
$y_{ss}[4]$	45.33	2.03×10^4	2.02×10^4
$y_{sr}[1]$	710.74	1.11×10^4	1.08×10^3
$y_{sr}[2]$	824.49	1.44×10^4	5.07×10^4
$y_{sr}[3]$	593.59	7.86×10^3	2.82×10^4
$y_{sr}[4]$	901.54	4.91×10^4	3.35×10^4
$y_{sr}[5]$	974.77	7.06×10^4	2.13×10^5

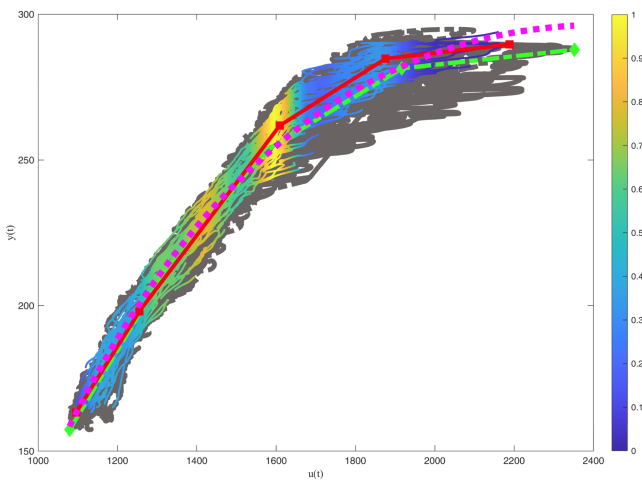


Fig. 7. Density plot of the special data samples, $\hat{F}(u(t))$ (red solid) from the proposed method, $\hat{F}_h(u(t))$ (green dashdot) from the Hammerstein identification method, and $\hat{F}_s(u(t))$ (magenta dot) from the sparse identification method.

the data fluctuates frequently at high power values, and the flow characteristics of regulating valves demonstrate a nonnegligible nonlinearity. The density plot of the special data samples in Ψ_{us} and Ψ_{ys} , as well as the nonlinear models $\hat{F}(u(t))$, $\hat{F}_h(u(t))$, and $\hat{F}_s(u(t))$, respectively, are estimated by the proposed method; the Hammerstein identification method and the sparse identification method are both given in Fig. 7. It can be seen that the nonlinear models estimated by the three methods are close at low values of $y(t)$, but have large differences at high values of $y(t)$.

A common practice for model validation is to evaluate how an identified model performs for different data [36]. To validate the estimated model in Fig. 7, other ten days of new samples of $u(t)$ in Fig. 8 are taken as the input into $\hat{F}(u(t))$ to obtain the simulated output $\hat{y}(t)$. The validity of $\hat{F}(u(t))$ can be verified by comparing $\hat{y}(t)$ with the special segments in the measured output $y(t)$ without estimating the dynamic system $G_i(p)$. For the Hammerstein identification method, the simulated output is $\hat{y}_h(t) = \hat{G}_h(p)\hat{F}_h(u(t))$, which is obtained by the estimated nonlinear submodel $\hat{F}_h(u(t))$ and the single linear dynamic

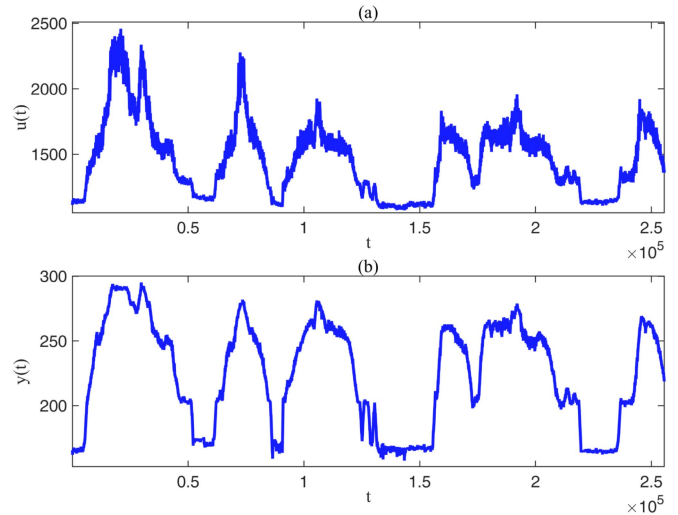


Fig. 8. Other ten days of new data samples for model validation: (a) $u(t)$ (blue dot), (b) $y(t)$ (blue dot).

submodel $\hat{G}_h(p)$. For the sparse identification method, the simulated output is obtained by integrating $\hat{\mathbf{Y}} = \Theta(\mathbf{W})\hat{\Xi}$. Some time sequences for model comparison are shown in Fig. 9, where $\hat{y}_{ss}[m]$ and $\hat{y}_{sr}[l]$ are marked with orange dot boxes and green dot boxes, respectively.

The simulated output $\hat{y}(t)$ is close to $y(t)$ in the presence of strong noise, especially in special segments, indicating that the nonlinear model $\hat{F}(u(t))$ estimated by the proposed method is accurate. The simulated outputs $\hat{y}_h(t)$ and $\hat{y}_s(t)$ of the Hammerstein identification method and the sparse identification method, respectively, have a large difference with $y(t)$ in the steady-state segments and slope-response segments, as shown by the orange and green dot boxes in the Fig. 9(b), (d), and (f). Table III lists the mean squared errors of three methods for the special segments in Fig. 9, where the values calculated by the two comparison methods are much larger than those for the proposed method. Paired-sample t tests [38] are performed on the special segments in Table III. For example, the t value of $\hat{y}_{ss}[1]$ obtained by the proposed method and the steady-state segment $y_{ss}[1]$ is 1.87, less than the critical value 1.964 under $\alpha = 0.05$ level. The null hypothesis is accepted, i.e., the mean of the sample differences between $y_{ss}[1]$ and $\hat{y}_{ss}[1]$ is 0. By contrast, for the two comparison methods, the calculated t values of $\hat{y}_{h,ss}[1]$ and $\hat{y}_{s,ss}[1]$ are 102.31 and 79.93, failing the paired-sample t test. The validation result clearly supports the effectiveness of the proposed method.

The Hammerstein identification method and the sparse identification method fail because they ignore the changes in the dynamics of steam turbines and generators at different operating points. As a proof, Fig. 10 confirms the presence of these changes by showing some data samples of $\hat{x}(t)$ and $y(t)$ under low and high values of $y(t)$. Clearly, the dynamics at low [marked as the box I in Fig. 10(a)] and high [marked as the box II in Fig. 10(b)] values of $y(t)$ are quite different, which will inevitably affect the estimation of the nonlinear model of flow characteristics of main steam regulating valves.

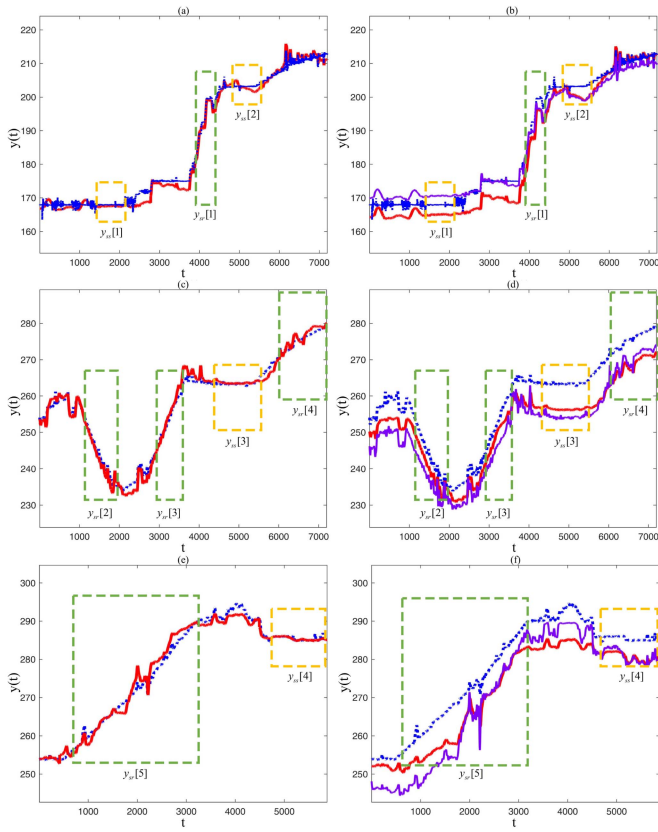


Fig. 9. Validation of $\hat{F}(u(t))$ from the proposed method (left column): measured output $y(t)$ (blue dot), simulated output $\hat{y}(t)$ (red solid), steady-state segments $\hat{y}_{ss}[m]$ with $m = 1, \dots, 4$ (orange dot boxes), and slope-response segments $\hat{y}_{sr}[l]$ with $l = 1, \dots, 5$ (green dot boxes); the validation of $\hat{F}_h(u(t))$ and $\hat{F}_s(u(t))$ from the Hammerstein identification method and the sparse identification method (right column): $y(t)$ (blue dot), $\hat{y}_h(t)$ (red solid) and $\hat{y}_s(t)$ (purple solid).

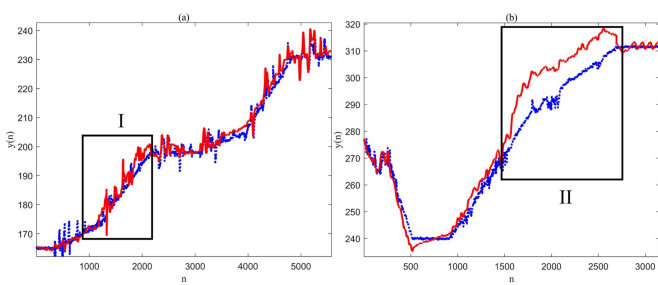


Fig. 10. Data samples $\hat{y}(t)$ (red solid) and $y(t)$ (blue dot) under different operating points: (a) the low value of $y(t)$ in the range [167.7 MW, 202.3 MW], marked as the box I, (b) the high value of $y(t)$ in the range [267.4 MW, 314.9 MW], marked as the box II.

A simulation investigation is implemented to illustrate the necessity of separating nonlinear flow characteristics from the dynamics of steam turbines and generators at different operating points. Consider the same structured system depicted in Fig. 1, where the nonlinear model $F(u(t))$ is similar to the estimated

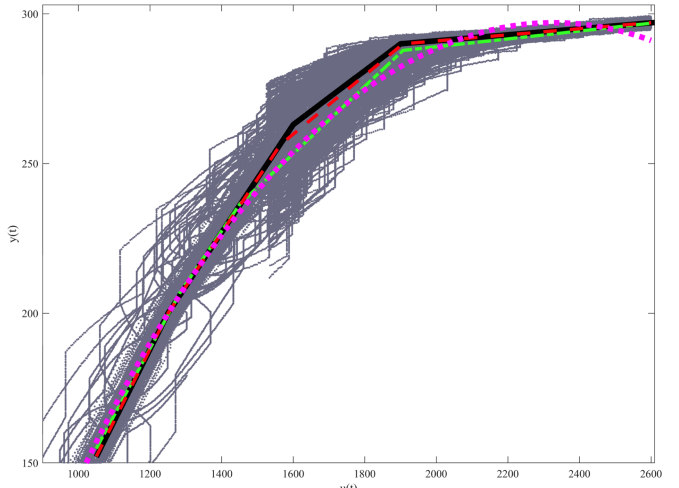


Fig. 11. Data samples in simulation investigation (gray dot), true model $F(\cdot)$ (black solid), $\hat{F}(u(t))$ (red dash) from the proposed method, $\hat{F}_h(u(t))$ (green dashdot) from the Hammerstein identification method, and $\hat{F}_s(u(t))$ (magenta dot) from the sparse identification method.

TABLE IV
IDENTIFICATION RESULTS OF THE PROPOSED METHOD AND THE HAMMERSTEIN IDENTIFICATION METHOD

Method	j	$\tilde{K}_{f,j}$	$K_{f,j}$	\tilde{C}_j	C_j	$[\hat{u}_j, \hat{u}_{j+1}]$
The proposed method	1	0.239	0.24	-99.052	-100	[1050, 1251]
	2	0.179	0.18	-24.078	-25	[1251, 1564]
	3	0.098	0.09	102.60	119	[1564.1, 1907]
	4	0.010	0.01	270.477	271	[1907, 2595]
The Hammerstein identification method	1	0.177	0.24	-20.242	-100	[1050, 1282]
	2	0.113	0.18	73.315	-25	[1282, 1451.7]
	3	0.017	0.09	255.814	119	[1451.7, 1906.8]
	4	0.010	0.01	271.966	271	[1906.8, 2600]

nonlinear model in (30)

$$F(u(t)) = \begin{cases} 0.24 \cdot u(t) - 100, & 1050 \leq u(t) < 1250 \\ 0.18 \cdot u(t) - 25, & 1250 \leq u(t) < 1600 \\ 0.09 \cdot u(t) + 119, & 1600 \leq u(t) < 1900 \\ 0.01 \cdot u(t) + 271, & 1900 \leq u(t) < 2600 \end{cases}.$$

Two continuous-time linear dynamic submodels $G_1(s)$ and $G_2(s)$ working at the different operating points are considered

$$G_1(s) = \frac{1}{10s + 1} e^{-3s}, \quad G_2(s) = \frac{1}{80s + 1} e^{-10s} \quad (31)$$

where the time constants and delay times of $G_1(s)$ and $G_2(s)$ have significant differences at low and high power values.

The simulation is executed with the sampling period $h = 1$ sec, and the total length of the simulation is ten days. The estimated nonlinear model from the three methods are compared in Fig. 11. Table IV presents the estimated nonlinear parameters from the proposed method and the Hammerstein identification method. For the sparse identification method, the library of candidate nonlinear functions is the same as in the above industrial case study. As revealed in Fig. 11, $\hat{F}_h(u(t))$ estimated by the Hammerstein identification method and $\hat{F}_s(u(t))$ estimated by the sparse identification method deviate from the true model $F(u(t))$, especially at high power values with large dynamic

changes. The estimated parameters of $\hat{F}_h(u(t))$ in Table IV are quite different from the true values. By contrast, the special segments do not contain dynamic information, so the nonlinear model $\hat{F}(u(t))$ estimated by the proposed method is very close to $F(u(t))$ over the entire operating range. This is confirmed in Table IV where the estimated parameters of $\hat{F}(u(t))$ are close to the true values.

V. CONCLUSION

This article proposed a new method to identify nonlinear flow characteristics of main steam regulating valves by exploiting special segments in historical data. The special segments referred to steady-state segments with constant amplitudes and slope-response segments with large amplitude changes, both of which could be automatically extracted by exploiting a piecewise linear representation technique. The linear relationships between the special segments and the nonlinear model parameters were theoretically established. The nonlinear model of flow characteristics was isolated from the dynamic process of steam turbines and generators based on the special segments, and the nonlinear model parameters were estimated by a linear dynamic programming algorithm. In the industrial case studies, the proposed method achieved an accurate estimation of the nonlinear flow characteristics of regulating valves, while the Hammerstein identification method and the sparse identification method gave biased results because of ignoring the variations in dynamic characteristics at different operating points. The nonlinear model identified based on the proposed method can compensate the primary frequency control response performance. The compensation scheme will be investigated in thermal power generation units as future work.

REFERENCES

- [1] G. Wen, G. Hu, J. Hu, X. Shi, and G. Chen, "Frequency regulation of source-grid-load systems: A compound control strategy," *IEEE Trans. Ind. Inform.*, vol. 12, no. 1, pp. 69–78, Feb. 2016.
- [2] H. Berahmandpour, S. M. Kouhsari, and H. Rastegar, "A new flexibility based probabilistic economic load dispatch solution incorporating wind power," *Int. J. Elect. Power Energy Syst.*, vol. 135, Feb. 2022, Art. no. 107546.
- [3] J. Rua, A. Verheyen, J. Jaschke, and L. O. Nord, "Optimal scheduling of flexible thermal power plants with lifetime enhancement under uncertainty," *Appl. Thermal Eng.*, vol. 191, pp. 116794, Jun. 2021.
- [4] F. Hong et al., "A new assessment mechanism of primary frequency regulation capability for a supercritical thermal power plant in deep peaking," *Energy Sci. Eng.*, vol. 11, pp. 547–564, Nov. 2023.
- [5] J. Wang and Q. Zhang, "Detection of asymmetric control valve stiction from oscillatory data using an extended Hammerstein system identification method," *J. Process Control*, vol. 24, no. 1, pp. 1–12, Jan. 2014.
- [6] C. R. Rad and O. Hancu, "An improved nonlinear modelling and identification methodology of a servo-pneumatic actuating system with complex internal design for high-accuracy motion control applications," *Simul. Model. Pract. Theory*, vol. 75, pp. 29–47, Jun. 2017.
- [7] H. Zhang, M. Gao, H. Yu, H. Fan, and J. Zhang, "A dynamic nonlinear model used for controller design of a 600 MW supercritical circulating fluidized bed boiler-turbine unit," *Appl. Thermal Eng.*, vol. 212, Jul. 2022, Art. no. 118547.
- [8] J. Qian, C. Hou, J. Wu, Z. Gao, and Z. Jin, "Aerodynamics analysis of superheated steam flow through multi-stage perforated plates," *Int. J. Heat Mass Transf.*, vol. 141, pp. 48–57, Oct. 2019.
- [9] D. Wang, D. Liu, C. Wang, Y. Zhou, X. Li, and M. Yang, "Flexibility improvement method of coal-fired thermal power plant based on the multi-scale utilization of steam turbine energy storage," *Energy*, vol. 239, Jan. 2022, Art. no. 122301.
- [10] L. Fang and J. Wang, "Identification of hammerstein systems using Preisach model for sticky control valves," *Ind. Eng. Chem. Res.*, vol. 54, no. 3, pp. 1028–1040, Jan. 2015.
- [11] R. B. di Capaci, M. Vaccari, C. Scali, and G. Pannocchia, "Enhancing MPC formulations by identification and estimation of valve stiction," *J. Process Control*, vol. 81, pp. 31–39, Sep. 2019.
- [12] P. D. Delou, J. Matias, J. Jaschke, M. B. de Souza Jr, and A. R. Secchi, "Steady-state real-time optimization using transient measurements and approximated Hammerstein dynamic model: A proof of concept in an experimental rig," *J. Process Control*, vol. 132, pp. 103111, Dec. 2023.
- [13] S. L. Brunton, J. L. Proctor, and J. N. Kutz, "Discovering governing equations from data by sparse identification of nonlinear dynamical systems," *Proc. Natl. Acad. Sci. USA*, vol. 113, no. 15, pp. 3932–3937, Mar. 2016.
- [14] Z. Chen, Y. Liu, and H. Sun, "Physics-informed learning of governing equations from scarce data," *Nat. Commun.*, vol. 12, no. 1, Oct. 2021, Art. no. 6136.
- [15] J. Li, X. Li, H. T. Zhang, G. Chen, and Y. Yuan, "Data-driven discovery of block-oriented nonlinear models using sparse null-subspace methods," *IEEE Trans. Cybern.*, vol. 52, no. 5, pp. 3794–3804, May 2022.
- [16] F. Giri and E. W. Bai, *Block-Oriented Nonlinear System Identification*, London, U.K.: Springer, 2010.
- [17] H. Salhi and S. Kamoun, "A recursive parametric estimation algorithm of multivariable nonlinear systems described by Hammerstein mathematical models," *Appl. Math. Model.*, vol. 39, no. 16, pp. 4951–4962, Aug. 2015.
- [18] P. Zhou, H. Song, H. Wang, and T. Chai, "Data-driven nonlinear subspace modeling for prediction and control of molten iron quality indices in blast furnace ironmaking," *IEEE Trans. Control Syst. Technol.*, vol. 25, no. 15, pp. 1761–1774, Sep. 2017.
- [19] B. Lyu, L. Jia, and F. Li, "Neuro-fuzzy based identification of Hammerstein OEAR systems," *Comput. Chem. Eng.*, vol. 141, Oct. 2020, Art. no. 106984.
- [20] G. T. Naozuka, H. L. Rocha, R. S. Silva, and R. C. Almeida, "SINDY-SA framework: Enhancing nonlinear system identification with sensitivity analysis," *Nonlinear Dyn.*, vol. 110, no. 3, pp. 2589–2609, Nov. 2022.
- [21] T. Tripura and S. Chakraborty, "A sparse bayesian framework for discovering interpretable nonlinear stochastic dynamical systems with Gaussian white noise," *Mech. Syst. Signal Process.*, vol. 187, May 2023, Art. no. 109939.
- [22] N. Pathak, T. S. Bhatti, and A. Verma, "Discrete data AGC of hydrothermal systems under varying turbine time constants along with the power system loading conditions," *IEEE Trans. Ind. Appl.*, vol. 53, no. 5, pp. 4998–5013, Sep./Oct. 2017.
- [23] L. Yao and Z. Ge, "Industrial Big Data modeling and monitoring framework for plant-wide processes," *IEEE Trans. Ind. Inform.*, vol. 17, no. 9, pp. 6399–6408, Sep. 2021.
- [24] L. Ren, T. Wang, Y. Laili, and L. Zhang, "A data-driven self-supervised LSTM-DeepFM model for industrial soft sensor," *IEEE Trans. Ind. Inform.*, vol. 18, no. 9, pp. 5859–5869, Sep. 2022.
- [25] J. Hou, F. Chen, P. Li, and Z. Zhu, "Gray-box parsimonious subspace identification of Hammerstein-type systems," *IEEE Trans. Ind. Electron.*, vol. 68, no. 10, pp. 9941–9951, Oct. 2021.
- [26] J. Wang, M. Wei, and X. Xing, "Static gain estimation for nonlinear dynamic systems from steady-state values hidden in historical data," *ISA Trans.*, vol. 120, pp. 78–88, Jan. 2022.
- [27] K. J. Astrom and K. Eklund, "A simple non-linear drum boiler model," *Int. J. Control.*, vol. 22, pp. 739–740, Aug. 1975.
- [28] D. E. Seborg, T. F. Edgar, and D. A. Mellichamp, *Process Dynamics and Control*, Hoboken, NJ, USA: Wiley, 2004.
- [29] E. Keogh, S. Chu, D. Hart, and M. Pazzani, "Segmenting time series: A survey and novel approach," in *Data Mining in Time Series Databases*, Singapore: World Scientific, 2004.
- [30] J. Wang, X. Pang, S. Gao, Y. Zhao, and S. Cui, "Assessment of automatic generation control performances of coal-fired power generation units based on amplitude changes," *Int. J. Elect. Power Energy Syst.*, vol. 108, pp. 19–30, Jun. 2019.
- [31] R. Bellman and R. Roth, "Curve fitting by segmented straight lines," *J. Amer. Statist. Assoc.*, vol. 64, pp. 1079–1084, Apr. 1969.
- [32] B. Zhou, H. Ye, H. Zhang, and M. Li, "A new qualitative trend analysis algorithm based on global polynomial fit," *AIChE J.*, vol. 63, no. 8, pp. 3374–3383, Mar. 2017.

- [33] I. Chivers and J. Sleighholme, "An introduction to algorithms and the Big O. Notation," in *Introduction to Programming with Fortran*, Cham, Switzerland: Springer, 2015.
- [34] D. Bertsekas, *Dynamic Programming and Optimal Control*, NH, USA: Athena Scientific, 2012.
- [35] J. M. Wooldridge, *Introductory Econometrics: A Modern Approach*, Boston, MA, USA: Cengage Learning, 2015.
- [36] L. Ljung, *System Identification: Theory for the User*, 2nd ed., Englewood Cliffs, NJ, USA: Prentice Hall, 1999.
- [37] L. Ljung, *System Identification Toolbox: User's Guide*. The Math Works, Inc, 2020, Available: www.mathworks.com/help/pdfdoc/identug.pdf
- [38] A. Ross and V. L. Willson, "Paired samples T-test," in *Basic and Advanced Statistical Tests*, Rotterdam, The Netherlands: SensePublishers: Brill, 2017.



Xiaotong Xing received the B.E. degree, in 2018, in automation from the Shandong University of Science and Technology, Shandong, China, where she is currently working toward the Ph.D. degree in control science and engineering with the College of Electrical Engineering and Automation.

Her research interests include model identification of nonlinear systems.



Peng Wei received the B.E. degree in automation from the Harbin University of Science and Technology (Rong Cheng), Shandong, Harbin, China, in 2019, and the M.Sc. degree in electrical engineering from the Shandong University of Science and Technology, Shandong, China, in 2022.

His research interests include process model modeling.



Song Gao received the B.E. degree in automatic control and the M.Sc. degree in control science and engineering from Xi'an Jiaotong University, Xi'an, China, in 2007 and 2010, respectively.

Since 2010, he has been with the Shandong Electric Power Research Institute, Jinan, China, where he is currently a Senior Engineer. His current research interests include automatic control, process monitoring and management for thermal power plants, and electric power grids.



Jiandong Wang (Senior Member, IEEE) received the B.E. degree in automatic control from Beijing University of Chemical Technology, Beijing, China, in 1997, and the M.Sc and Ph.D. degrees in electrical and computer engineering from the University of Alberta, Edmonton, Canada, in 2003 and 2007, respectively.

From 1997 to 2001, he was a Control Engineer with the Beijing Tsinghua Energy Simulation Company, Beijing, China. From 2006 to 2006, he was a Visiting Scholar with the Department of System Design Engineering, Keio University, Tokyo, Japan.

From 2006 to 2016, he was an Assistant/Associate/Full Professor with the College of Engineering, Peking University, Beijing, China. He is currently a Professor with the College of Electrical Engineering and Automation, Shandong University of Science and Technology, Qingdao, China. His research interests include industrial alarm systems, process monitoring, system identification, and their applications to industrial problems.

Dr. Wang was an Associate Editor for *Systems and Control Letters*, and *Journal of Franklin Institute*.



Xiangkun Pang received the M.Sc degree in control theory and control engineering from Shandong University, Jinan, China, in 2008.

He works with the Shandong Electric Power Research Institute, Jinan, China. His research interests include debugging and research of thermal automatic control systems for thermal power units, and research and development of network source coordination technology.